The Golgi ribbon structure facilitates anterograde transport of large cargoes

Gregory Lavieu, Myun Hwa Dunlop*, Alexander Lerich*, Hong Zheng, Francesca Bottanelli*, and James E. Rothman
Department of Cell Biology, Yale University School of Medicine, New Haven, CT 06520

ABSTRACT **In mammalian cells, individual Golgi stacks fuse laterally to form the characteristic perinuclear ribbon structure. Yet the purpose of this remarkable structure has been an enigma. We report that breaking down the ribbon of mammalian cells strongly inhibits intra-Golgi transport of large cargoes without altering the rate of transport of smaller cargoes. In addition, insect cells that naturally harbor dispersed Golgi stacks have limited capacity to transport artificial oversized cargoes. These results imply that the ribbon structure is an essential requirement for transport of large cargoes in mammalian cells, and we suggest that this is because it enables the dilated rims of cisternae (containing the aggregates) to move across the stack as they transfer among adjacent stacks within the ribbon structure.**

Monitoring Editor
Benjamin S. Glick
University of Chicago

Received: Apr 22, 2014
Revised: Jul 25, 2014
Accepted: Jul 31, 2014

INTRODUCTION

Although eukaryotic cells share membrane compartmentalization and many aspects of the secretory pathway, they also harbor differences. The organization of the Golgi apparatus is one example. In the yeast *Saccharomyces cerevisiae*, the Golgi is constituted of distant single cisternae (Franzusoff *et al.*, 1991); in flies, the Golgi is constituted of stacks dispersed throughout the cytoplasm (Kondylis and Rabouille, 2003); and, finally, in mammals, the Golgi stacks are concentrated at the perinuclear area, where they form a ribbon structure that results from the lateral fusion of many individual Golgi stacks (Ladinsky *et al.*, 1999). Although the Golgi ribbon has a function during the cell cycle (Rabouille and Kondylis, 2007), it is unclear why a ribbon is needed during secretion in interphase cells. Why do mammals harbor such a complex Golgi architecture, when the individual and disconnected Golgi cisternae of yeast seem to be as efficient in secreting proteins? This question is especially vexing, because the transport of secretory proteins is generally not affected when the ribbon structure in mammalian cells is disrupted to produce numerous individual Golgi stacks (Rogalski *et al.*, 1984; Van De Moortele *et al.*, 1993; Cole *et al.*, 1996; Trucco *et al.*, 2004).

Many mechanisms for intra-Golgi transport have been proposed (Glick and Luini 2011), the two most extreme being the maturation and the vesicular models. The main limitation of the vesicular model is that specialized cargoes (such as certain collagens) are too large to be accommodated by typical transport vesicles such as coatomer proteins I (COPI) vesicles (~70-nm internal diameter). One possibility, which we explore here, is that the ribbon structure serves the special purpose of facilitating the anterograde transport of such large cargoes.

We have shown that forward flow of large aggregated cargoes through the Golgi requires their concentration within the enlarged rims of Golgi cisternae and that they remain in the close vicinity of the cisternae during anterograde transport (Volchuk et al., 2000; Lavieu *et al.*, 2013; Pellett *et al.*, 2013); this process differs fundamentally from the transport of small cargoes, which seems to mainly utilize diffusible carriers (Pellett *et al.*, 2013). We speculated that aggregate transport may instead occur by a proposed process of "rim progression," in which the large cargo–laden rim of one cisterna may be itself transferred to another cisterna in a process of membrane fission–fusion. A process of rab conversion occurring vectorially across the Golgi stack (envisioned in an analogous model termed "cisternal progenitor" [Pfeffer, 2010]) could provide a ready mechanism to drive rim progression. In these models (Pfeffer, 2010; Lavieu *et al.*, 2013; Mironov *et al.*, 2013), contact between adjacent stacks within the ribbon should be required for efficient transport of large cargoes (but not small cargoes, which are accommodated within COPI vesicles or potentially in tubules of similar diameter).

This article was published online ahead of print in MBoC in Press (http://www.molbiolcell.org/cgi/doi/10.1091/mbc.E14-04-0931) on August 7, 2014.

*These authors participated equally in this work.

Address correspondence to: Gregory Lavieu (gregory.lavieu@yale.edu) or James E. Rothman (james.rothman@yale.edu).

Abbreviations used: CHX, cycloheximide; EM, electron microscopy; ER, endoplasmic reticulum; FBS, fetal bovine serum; GFP, green fluorescent protein; HBSS, Hanks' balanced salt solution; hGH, human growth hormone; KD, knockdown; NIH, National Institutes of Health; siRNA, small interfering RNA; STED, stimulated emission depletion; TCA, trichloroacetic acid; vWF, von Willebrand factor.

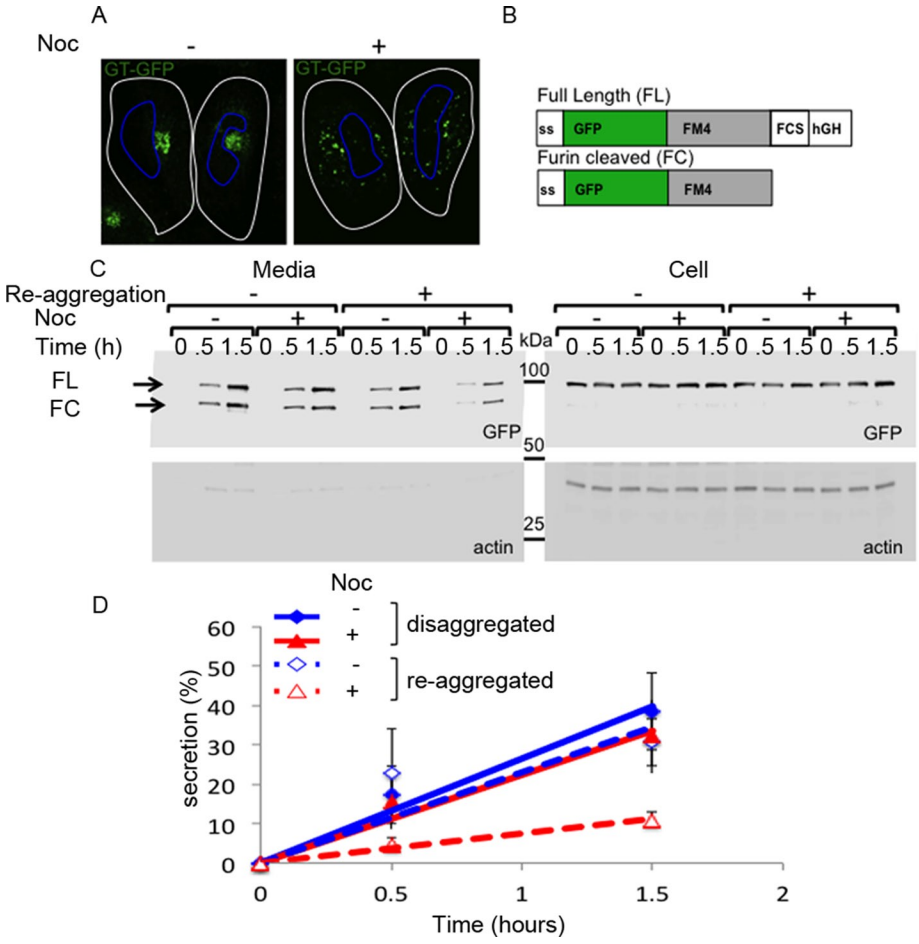

FIGURE 1: Nocodazole disrupts the ribbon and inhibits aggregates secretion. (A) Confocal micrographs illustrate nocodazole-induced Golgi ribbon disruption. HeLa cells expressing GT-GFP were treated or not with nocodazole (2 h, 1 µg/ml) before being prepared for confocal imaging. (B) Schematic representation of the drug-controlled aggregate. The human growth hormone (hGH) is fused to a signal sequence (ss), a GFP, four repeats of the self-aggregating FM domain (FM4), and a furin cleavage site that is cleaved during flow through the *trans*-Golgi network (TGN). (C) Immunoblots show the inhibition of aggregate secretion under nocodazole treatment. Cells expressing ssGFP-FM4-hGH were pretreated with nocodazole (2 h), which was maintained during the rest of the experiment. Then the temperature was shifted to 16°C in the presence of the disaggregating drug (1 h and 30 min, 1 µM). When required, the drug was removed to trigger reaggregation (30 min). Media was removed and replaced with fresh media containing or not the disaggregating drug. Temperature was shifted to 37°C and the media were collected at the indicated time points and submitted for TCA precipitation while the cells were harvested. Unless mentioned otherwise, all chase experiments were performed in the presence of CHX. TCA-precipitated media and cell lysate fractions were analyzed by SDS–PAGE/immunoblotting, which was followed by densitometry measurement. (D) Graph represents the percent of secretion over time for each condition. Data represent the mean ± SD of three independent experiments.

Thus rim progression and similar models make the striking prediction that disruption of the ribbon should selectively prevent anterograde transport of large but not small cargoes. In this study, we tested this prediction in a variety of different and complementary ways.

RESULTS

Nocodazole treatment inhibits the secretion of artificial aggregates

To test whether Golgi ribbon fragmentation affects intra-Golgi transport, we used nocodazole, a drug that prevents microtubule polymerization and that is well known to break down the Golgi ribbon of many cells into dispersed ministacks (Thyberg and Moskalewski, 1985; Cole *et al.*, 1996).

First, we combined nocodazole treatment with a drug-controlled aggregation system that allows for positioning soluble aggregates at different stages of the secretory pathway (Volchuk *et al.*, 2000; Lavieu *et al.*, 2013). The chimeric cargo is constituted of a signal sequence fused to a fluorescent protein, four repeats of the self-aggregation domain (FM4), a furin cleavage site, and the sequence encoding the human growth hormone (Figure 1B). In the absence of the disaggregating drug, the chimeric protein is aggregated and stays in the endoplasmic reticulum (ER). In the presence of the drug, at 16°C for 2 h, the now-disaggregated protein reaches the *cis* face of the Golgi, where it can be reaggregated by subsequent drug removal. Shifting the temperature back to 37°C in the absence or presence of the disaggregating drug allows for comparison of intra-Golgi transport and further secretion of large aggregated cargo versus small disaggregated cargo, respectively. Importantly, such a chase needs to be performed in the presence of cycloheximide (CHX), an inhibitor of protein synthesis.

We preincubated the cells for 2 h with nocodazole to disrupt the Golgi ribbon (Figure 1A) before manipulating the aggregation/positioning of the chimeric protein. Note that nocodazole as well as CHX were present during the entire course of the experiment, except if mentioned otherwise. The proteins were reaggregated or not within the *cis*-Golgi (using 16°C incubation), and then transport was resumed by shifting the temperature back to 37°C and we assessed the rate of secretion for each kind of cargo (Figure 1C). In the absence of nocodazole, aggregated and disaggregated cargoes showed similar rates of secretion, consistent with previous work. When the ribbon was broken by nocodazole, the secretion of aggregates that were prepositioned in the *cis*-Golgi was strongly inhibited (70% reduction), whereas the secretion of disaggregated cargo showed only a modest inhibition (15% reduction; Figure 1D).

We then assessed the intracellular localization of the nonsecreted fraction of the reaggregated protein using confocal microscopy. Working with nocodazole-induced ministacks allows for discriminating *cis*- from *trans*-Golgi cisternae, even at the light microscopy level (Dejgaard *et al.*, 2007). Within the very same cells, the localization of the green fluorescent protein (GFP)-tagged disaggregated or aggregated cargo was compared with a *cis*-Golgi marker (Gpp130 labeled with a red dye) and a *trans*-Golgi marker (p230 labeled with a far-red dye). As expected, *cis*- and *trans*-Golgi markers were easily distinguishable, as judged by the lack of overlay and the low

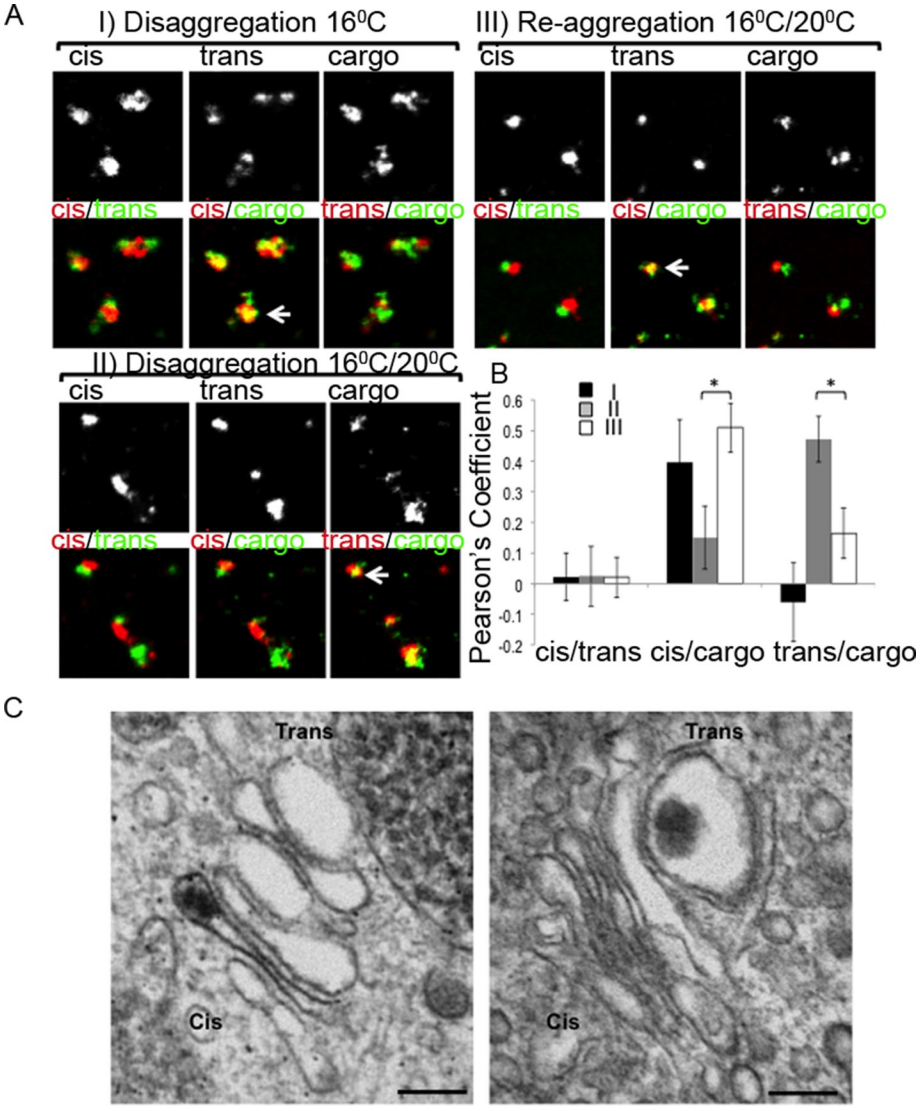

FIGURE 2: Nocodazole inhibits intra-Golgi transport of aggregates. (A) Confocal micrographs illustrate representative three-color imaged stacks containing aggregated or disaggregated cargoes. HT1080 cells stably expressing ssGFP-FM4-hGH were pretreated with nocodazole for 2 h. Nocodazole was maintained during the rest of the experiment. Cells were incubated at 16°C in the presence of the disaggregating drug (1 h, 30 min, 1 μM) to allow for positioning the cargo within the *cis*-Golgi (I). The disaggregating drug was removed (III) or not (II) for 30 min before the temperature was shifted to 20°C for 30 min. Cells were fixed and prepared for immunofluorescence against the *cis*-Golgi marker gpp130 (labeled with a red dye) and against the *trans*-Golgi marker p230 (labeled with a far-red dye). (B) Graph represents the Pearson's coefficient for each marker combination for each condition. For each condition, we analyzed between 70 and 150 ministacks. *, p values < 0.01. (C) Electron micrographs show the retention of aggregates within the *cis* face of nocodazole-induced stacks. After nocodazole pretreatment, HeLa cells expressing ssGFP-FM4-hGH were incubated at 16°C for 1 h, 30 min in presence of the disaggregating drug. The drug was then removed for 30 min to allow for reaggregation within the *cis* face of nocodazole-induced ministacks. The temperature was shifted to 20°C for 1 h, and cells were prepared for EM (left panel). As a positive control for *cis*→*trans* transport at 20°C, cells subjected to the same nocodazole treatment were incubated for 1 h with the disaggregating drug at 20°C, and reaggregation was triggered by drug removal for 30 min at 20°C to allow for visualization of the aggregates by conventional EM (right panel).

Pearson's coefficient value (Figure 2, A and B). At 16°C, the disaggregated cargo was specifically colocalizing with the *cis*-Golgi marker (Figure 2, A and B, condition I). When the cells were subsequently incubated at 20°C, a large portion of the disaggregated cargo reached the *trans*-Golgi (Figure 2, A and B, condition II), whereas the reaggregated cargo remained associated with the *cis*-Golgi cisternae (Figure 2, A and B, condition III). We observed the same *cis*-Golgi retention of the aggregates when the chase was performed at 37°C (Supplemental Figure S1).

These observations were qualitatively confirmed by electron microscopy (EM), which showed that aggregates prepositioned at the *cis* face of the nocodazole-induced ministack remained at the same position, even when the temperature was shifted to 20°C, which normally allows for *cis*→*trans* movement (Figure 2C, left panel). On the contrary, in the control condition, when reaggregation was triggered only at the end of the 20°C chase (in order to visualize the cargo by transmission EM), the cargo was now localized within the *trans*-Golgi (Figure 2C, right panel), made identifiable by its swollen aspect, which is typical at 20°C (Griffiths *et al*., 1989). This indicated again that disaggregated cargo passed through the ministacks, whereas the reaggregated cargo remained mostly within the *cis*-Golgi.

Nocodazole treatment inhibits the secretion of endogenous collagen I

The cargo used above was artificially aggregated and may not perfectly reflect the behavior of physiologically large cargoes. Collagen I, an abundant component of the extracellular matrix, is an example of a physiological large cargo (Ricard-Blum, 2011). We repeated our experiments using Saos-2 cells that secrete endogenous collagen I (Saito *et al*., 2009; Lavieu *et al*., 2013). We took advantage of the ascorbate-dependent folding of collagen to control the wave of collagen secretion (Harwood *et al*., 1976; Mironov et al., 2001). Cells were cultured overnight in ascorbate-depleted media to block collagen within the ER and then, during the last 2 h, cells were pretreated with nocodazole before ascorbate was added back to allow for collagen folding and subsequent exit from the ER. We then assessed the secretion of endogenous collagen I (large cargo) and endogenous MMP2 (small cargo) simultaneously within the same samples. This allows for the direct comparison of the secretion rates of the two endogenous cargoes using a bulk biochemical secretion assay that leaves no room for biased interpretation. The rate of secretion of collagen I was strongly diminished (70% reduction) in the presence of nocodazole, whereas the secretion of MMP-2 was not altered by more than 20% (Figure 3, A and B).

We then assessed the localization of collagen I within the ministacks by two-color stimulated emission depletion (STED) microscopy (Hell and Wichmann, 1994; Schill *et al*., 2013), which allows for

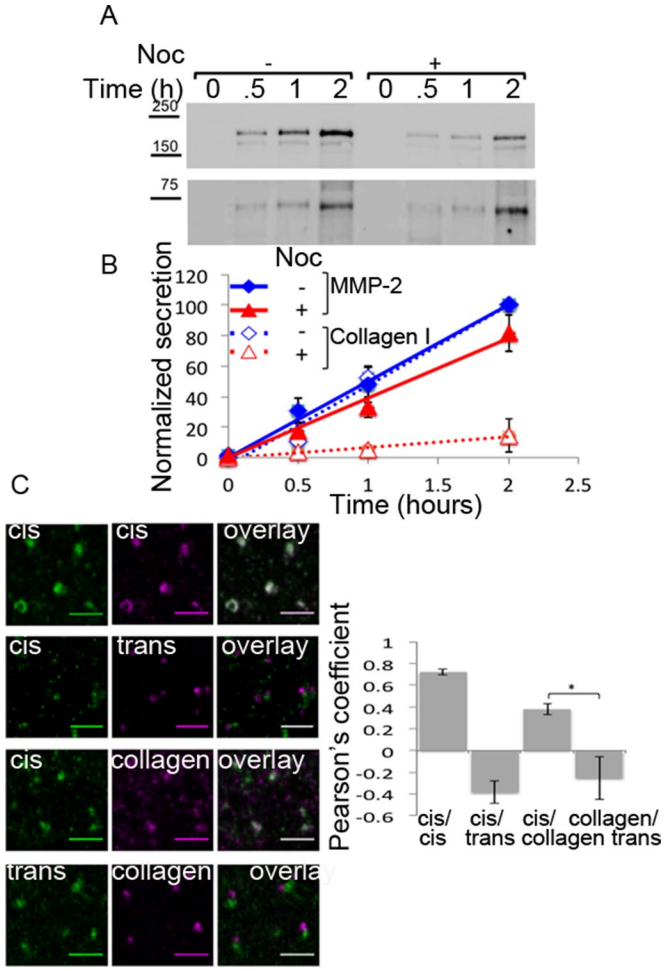

FIGURE 3: MMP-2 flows through nocodazole-induced stacks, whereas collagen I is retained within the *cis*-Golgi. (A) Immunoblots show the inhibition of collagen I secretion under nocodazole treatment. Saos-2 cells were incubated overnight in ascorbate-depleted media. During the last 2 h, cells were treated or not with nocodazole, which was maintained during the experiment. Chase was performed at 37°C in media containing ascorbate and CHX. TCA-precipitated media was analyzed by SDS–PAGE/immunoblotting, followed by densitometry measurement. (B) Graph represents the normalized percent of secretion over time for each condition. MMP-2 and collagen I secretions at 2 h were set to 100%. Data represent the mean ± SD of three independent experiments. (C) Two-color STED micrographs show that collagen I is retained at the *cis* face of Golgi ministacks. Saos2 cells were treated as described above, except that the chase was performed at 20°C for 1 h. Cells were fixed and prepared for immunofluorescence against collagen I and the *cis*-Golgi marker gpp130 or the *trans*-Golgi marker p230. Primary antibodies were detected with secondary antibodies coupled with STED-compatible dyes. Graph represents the Pearson's coefficient for each marker combination for each condition. Values represent the mean ± SD. For each condition, we analyzed between 67 and 83 ministacks. *, *p* values < 0.01.

~70-nm lateral resolution (Pellett *et al.*, 2011). This resolution is sufficient to discriminate *cis*- and *trans*-Golgi cisternae, which are typically separated by at least 200 nm. The cargo was found to colocalize more with the *cis*-Golgi marker than the *trans* marker regardless of performing the chase at 20 or 37°C (Figure 3C and Supplemental Figure S2). This suggests again that the flow of collagen though the Golgi ministack was inhibited, or at least slowed down.

A previous study reported that the classical cargo vsv-G and procollagen are both efficiently transported through nocodazole-induced stacks (Trucco *et al.*, 2004). Although our results agree with the results for the classical cargo, they diverge with regard to collagen transport. We do not have a full and rational explanation for this discrepancy, but we noted at least two major differences between the respective studies. First, the authors used a different cell type, and, more importantly, they added in their protocol a 40/15/40°C temperature shift cycle to control the cargo release wave, which implies that their intra-Golgi transport assay was performed at 40°C, when our experiments were conducted at either 20 or 37°C.

Grasp55/65 small interfering RNA (siRNA)-mediated ribbon disruption also inhibits rim progression

One interpretation of the results reported above would be to consider that the phenotype is mainly due to the alteration of the microtubule network and is only an indirect consequence of the ribbon breakdown. To test this hypothesis, we decided to knock down grasp55/65, which is known to disrupt the ribbon structure of the Golgi without affecting the microtubule organization (Puthenveedu *et al.*, 2006; Feinstein and Linstedt, 2008; Lee *et al.*, 2014). As judged by immunoblotting and immunofluorescence analysis (Figure 4, A–C), at least 75% of the grasp55/65 proteins were efficiently silenced within cells treated with specific siRNA. As previously reported (Feinstein and Linstedt, 2008), we confirmed that these cells harbored a mildly scattered Golgi (Figure 4A and graph), without showing any alteration of the microtubules (Figure S3).

First, we used the disaggregation/reaggregation assay and showed that grasp55/65 knockdown (KD) inhibited the secretion of *cis*-Golgi reaggregated cargo by a factor of two (Figure 4B, lanes 2 and 5), whereas the secretion of the disaggregated cargo was not decreased at all (Figure 4B, lanes 1 and 4) and even seemed to be slightly increased. Note that, in our hands, this increase was not statistically significant, although previous studies reported a robust 40% increase of the secretion of classical cargo under similar conditions (grasp55/65 KD; Xiang *et al.*, 2013).

We then tested whether the grasp55/65 KD had a similar effect on the secretion of large and small endogenous cargoes. Collagen I secretion was inhibited by 60% when grasp55/65 were silenced, whereas MMP-2 secretion was not diminished (Figure 4C). These results recapitulated the observations made under nocodazole treatment and suggest that the transport inhibition of large cargoes is directly due to the disruption of the ribbon structure. It is important to note that the grasp55/65 KD-mediated scattering of the Golgi is less pronounced than the nocodazole-mediated ribbon disruption. This may explain why the inhibition on large cargo transport mediated by grasp55/65 siRNA (≈50%) is less severe than the inhibition triggered by nocodazole (≈70%).

Fly cells harbor dispersed Golgi stacks and poorly secrete reaggregated cargo

Drosophila S2 cells naturally harbor Golgi stacks that are dispersed through the cytoplasm (Kondylis and Rabouille, 2003). As for microtubule-induced ministacks, *cis*- and *trans*-Golgi cisternae can be resolved at the light level (Figure 5A and graph). We first generated a plasmid compatible with the expression of the drug-controlled GFP aggregate within S2 cells. S2 cells normally grow at 25°C, and this prevented the direct application of the16°C reaggregation temperature block that we established with HeLa cells, which normally grow at 37°C. We empirically tested several lower temperatures to determine which one would be most appropriate to slow down trafficking of the disaggregated human growth hormone (hGH) cargo, such

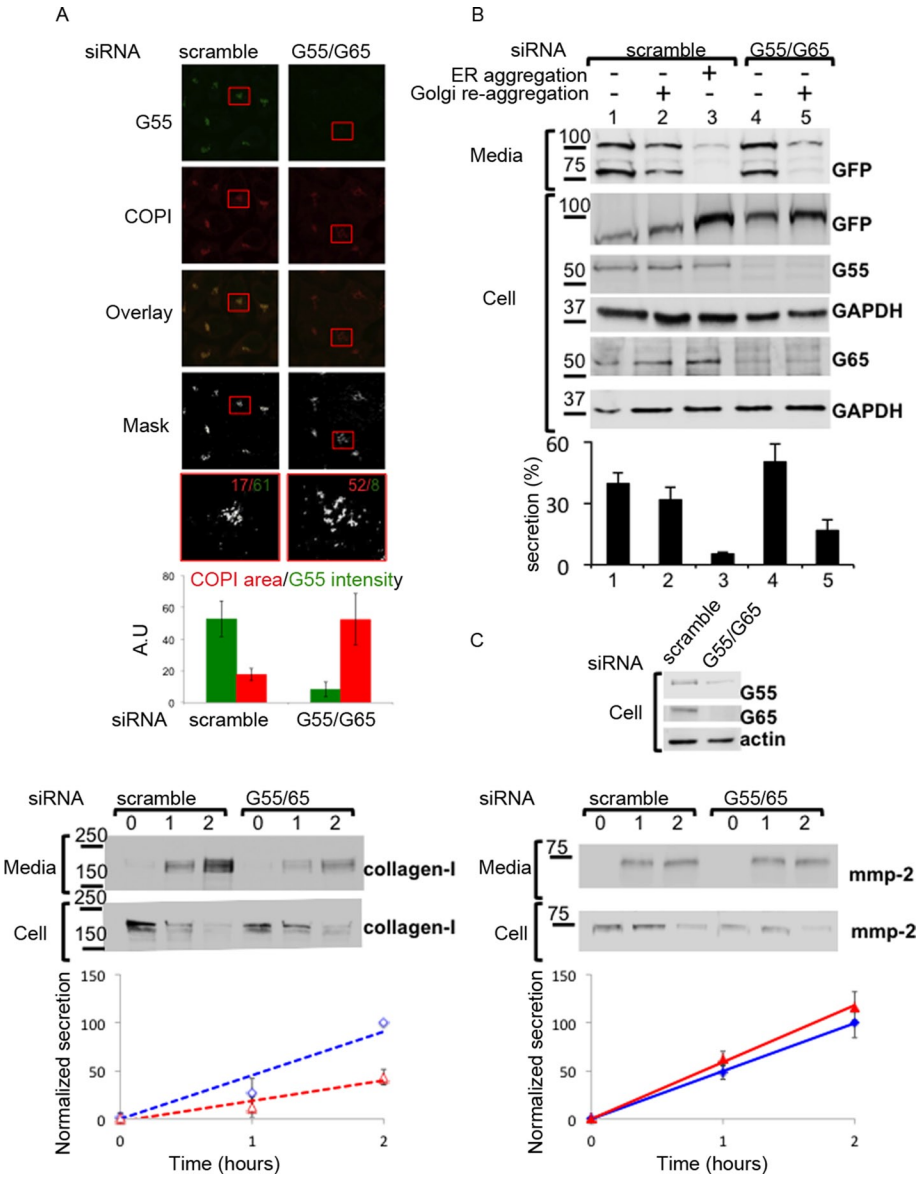

FIGURE 4: grasp55/65 silencing scatters the Golgi ribbon and inhibits the secretion of aggregates and collagen I. (A) Confocal micrographs illustrating the Golgi scattering mediated by grasp 55/65 silencing. HeLa cells were treated with either scrambled or grasp55/65 siRNA for 3 d. Cells were fixed and prepared for immunofluorescence against COPI (red channel) and Grasp55 (green channel). Using ImageJ, we delineated the Golgi shape within the red channel (mask). For each Golgi, we measured the Golgi area (within the red channel) to evaluate the Golgi scattering and the G55 intensity (within the green channel) to evaluate the efficiency of silencing. Red boxes show higher magnification of indicated Golgi. Graphs show Golgi scattering in red and G55 intensity in green for each condition. Values represent the mean ± SD of two independent experiments. For each condition, we analyzed at least 50 ministacks. (B) Immunoblots showing the inhibition of hGH secretion in grasp55/65-silenced cells. Cells expressing ssGFP-FM4-GFP were treated with grasp55/65 or scrambled siRNA for 3 d. Secretion of disaggregated and reaggregated cargo was then measured as described in Figure 1A (minus the nocodazole treatment) after a 2-h chase at 37°C. siRNA silencing efficiency was confirmed by immunoblot analysis against G55 and G65 within the cell fraction. Graph represents the percent of secretion for each condition. Data represent the mean ± SD of three independent experiments. (C) Immunoblots showing the inhibition of collagen I secretion in grasp55/65 silenced cells. Saos2 cells were treated with siRNA against G55/G65 for 3 d. siRNA silencing efficiency within Saos-2 cells was confirmed by immunoblot analysis (upper panel). MMP-2 and collagen I secretion were then assessed as described in Figure 3A (minus the nocodazole treatment). Graphs represent the normalized rate of secretion over time, for each condition. MMP-2 and collagen I secretion at 2 h were set to 100%. Data represent the mean ± SD of three independent experiments.

that it would be positioned within the *cis*-Golgi before its reaggregation was triggered. We found that, at 10°C, the disaggregated cargo reached the *cis*-Golgi after 5 min and then progressively reached the *trans*-Golgi within the next 20 min (Figure 5B and graph). Importantly, after 40 min at 10°C, the vast majority of the disaggregated cargo remained at the *trans*-Golgi (Figure 5B), and only a very small portion could be detected in the media (<5%, Figure 5C). We concluded that the 10°C incubation slowed down the trafficking within S2 cells and triggered retention of the cargo within the *trans*-Golgi, thereby mimicking the well-known 20°C temperature block often used in mammalian cells. Now knowing precisely the kinetics of the sequential ER→*cis*-Golgi→*trans*-Golgi transport at 10°C, we decided to incubate the S2 cells at 10°C for 5 min in the presence of the disaggregating drug to position the cargo within the *cis*-Golgi before triggering (or not) its reaggregation for 10 min on ice, which did not alter the microtubule network (Figure S4). The cells were then either incubated for 20–40 min at 10°C before being processed for confocal microscopy or were incubated at 20°C to analyze and compare the rate of secretion of each reaggregated and disaggregated cargo. As judged by confocal microscopy, the reaggregated cargo remained associated longer within the *cis*-Golgi (Figure 5D and graph; up to 40 min instead of 5–10 min for the disaggregated cargo). A portion of the aggregates reached the *trans*-Golgi, but again was more than two times slower than the disaggregated cargo. Analysis of the bulk secretion when transport was resumed at 20°C revealed that the secretion of the aggregates was inhibited by a factor of two when compared with the disaggregated cargo (Figure 5E and graph). Note that almost 100% of the disaggregated hGH was released from the S2 cells, whereas only 50% was released from the HeLa cells. We attribute this difference to the transfection efficiency and the protein overexpression level, which is considerably higher in HeLa cells than in S2 cells, resulting in a large portion of the ER aggregates remaining insensitive to the disaggregating drug in HeLa cells. This, however, has no impact on our interpretation of the results.

DISCUSSION

Our previous results (Volchuk *et al.*, 2000; Lavieu *et al.*, 2013; Pellett *et al.*, 2013) and the current results suggest that cargoes follow distinct secretory tracks within the Golgi according to their size. To explain these results (Figure 6), we propose that large

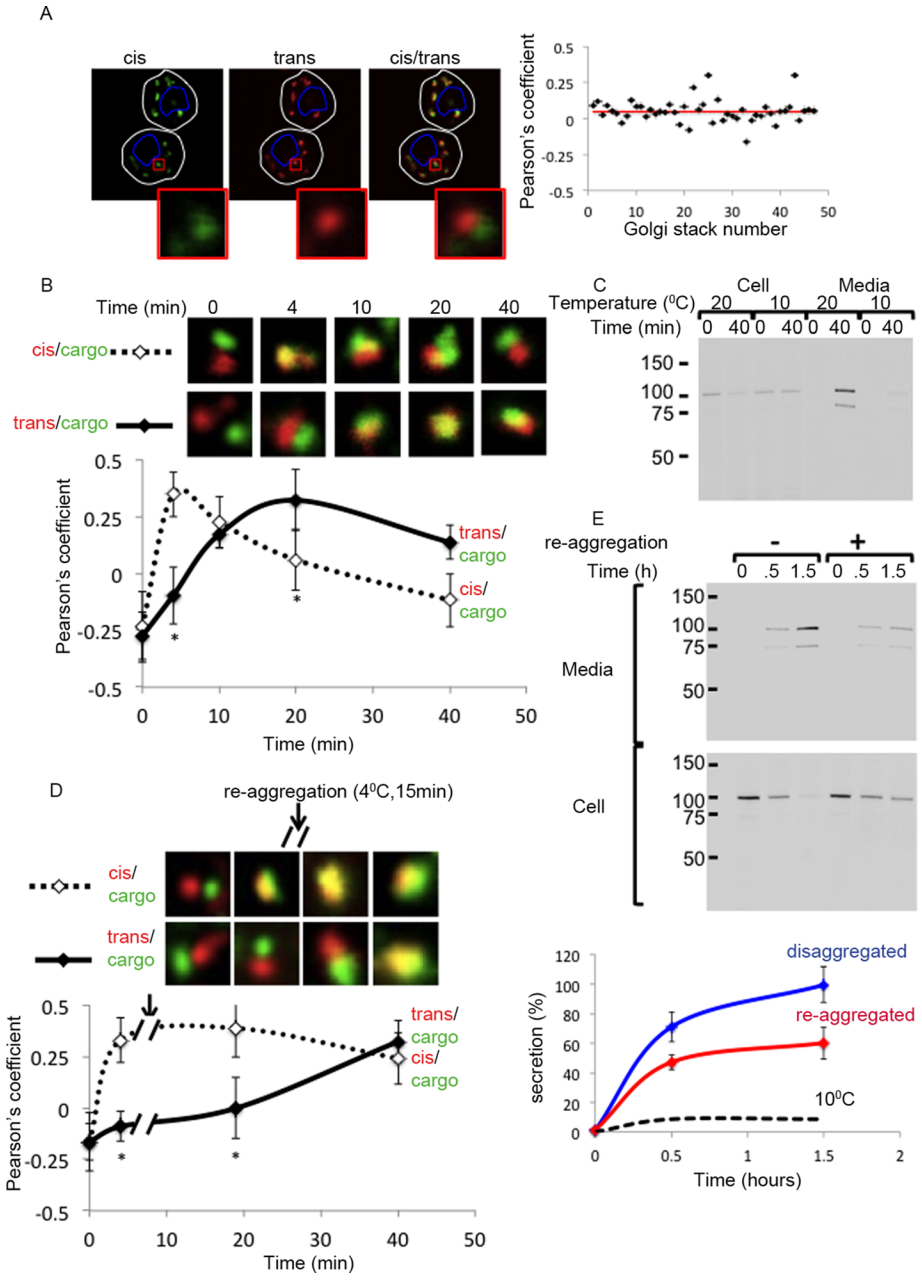

FIGURE 5: S2 cells poorly secrete aggregates, which are retained within the *cis*-Golgi. (A) Confocal micrograph showing separated *cis*- and *trans*-Golgi within single stacks through the cytoplasm of S2 cells. S2 cells were fixed and prepared for immunofluorescence against Gm130 (green-labeled *cis*-Golgi marker) and G245 (red labeled *trans*-Golgi marker). Graph shows Pearson's coefficient value for each imaged single Golgi stack. Red line represents the average value over 50 analyzed stacks. (B) Transport kinetics of disaggregated cargo at 10°C. The S2 cells expressing GFP-FM4-hGH were incubated at 10°C for various time points in the presence of the disaggregating drug, before being fixed and prepared for immunofluorescence against Gm130 (*cis*-Golgi) or G245 (*trans*-Golgi) labeled with a red dye, the green signal emanating from the GFP-tagged cargo. Confocal micrographs show representative Golgi stacks at each time point. Graph shows the Pearson's coefficient over time for each combination. Data represent the mean ± SD of three independent experiments. For each time point of each experiment, at least 30 stacks were analyzed. *, p values < 0.01. (C) Immunoblot showing the secretion block at 10°C. The S2 cells expressing GFP-FM4-hGH were incubated at 10 or 20°C for 0 or 40 min in the presence of the disaggregating drug. Media and cell contents were analyzed by immunoblot. (D) Confocal micrographs illustrate the inhibition of intra-Golgi transport of aggregates. As in B, cells were incubated at 10°C for 5 min in the presence of the disaggregating drug to position the cargo within the *cis*-Golgi. Then, reaggregation was triggered by drug removal (15 min on ice) before shifting the temperature back to 10°C for 20 or 40 min. Cells were then fixed and prepared for immunofluorescence as in B. Confocal micrographs show the transport kinetics of GFP aggregates within Golgi stacks labeled with *cis* or *trans* markers. Graph shows the Pearson's coefficient over time for each combination. Data represent the mean ± SD of two independent experiments. For each time point of each experiment, at least 30 stacks were analyzed. *, p values < 0.01. (E) Immunoblot shows the inhibition of aggregate secretion. Cells were treated as in C, except that after the 15-min reaggregation at 4°C, the temperature was shifted to 20°C with or without the drug to allow for secretion. Media and cell fractions were analyzed by immunoblot and densitometry. Graphs show the secretion over time for each condition. Data represent the mean ± SD of two independent experiments. The dashed line indicates the percent of secretion at 10°C for disaggregated cargo, as illustrated on the gel in B.

cargoes freshly arrived at the *cis*-Golgi are first concentrated at the enlarged rim of the *cis*-Golgi cisternae, where they are physically sequestered from other classical small cargoes. This separation, which remains to be further demonstrated, could simply result from the fact that large aggregates are too big to be accommodated within the narrow confines of the flattened central portions of the stacked cisternae. Fission of the enlarged rims may occasionally occur and would result in a more robust sequestration of the large cargo from the rest of the cisternae (Volchuk *et al.*, 2000). This may be the purpose of the so-called mega-vesicles, which have been reported to contain 20% of the soluble aggregates (Volchuk *et al.*, 2000), but in theory, the enlarged rims may remain physically connected to the cisternae in many cases. Making the assumption that the Golgi ribbon is going through continuous fission–fusion cycles, we propose that single stacks emanating from the ribbon and containing large cargoes within their *cis*-Golgi cisterna will fuse laterally with one another to form a new ribbon. When the fusion is homotypic (the *cis* cisterna of one stack fusing with the *cis* cisterna of an adjacent stack), no net anterograde movement occurs, though such an event many not be entirely unproductive because it could allow additional time for efficient posttranslational modification. However, when the lateral fusion is heterotypic (the *cis* cisterna of a stack containing the cargo fusing with the medial cisterna of the adjacent stack), this would allow for forward movement of the cargo into the next compartment and so on across the stack.

The Golgi ribbon (facilitated by microtubule-based motility of individual stacks) would ultimately be formed and maintained by a very dynamic process of fission–fusion

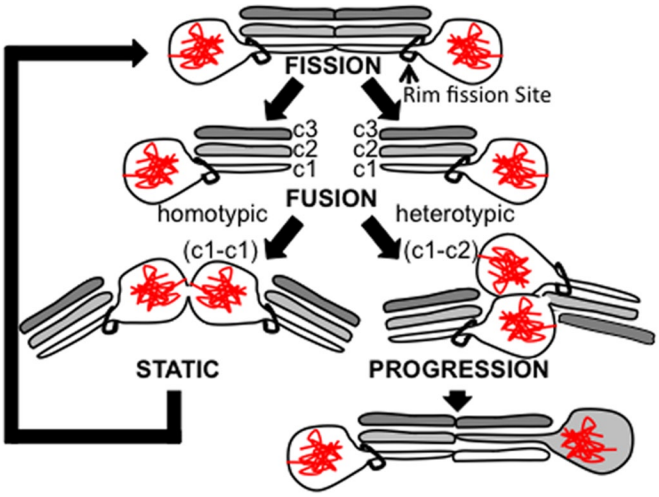

FIGURE 6: How the ribbon may facilitate rim progression: Ribbon and single stacks go through continuous fission–fusion cycles. *cis*-Golgi-localized aggregates concentrate at the rim of the cisterna of Golgi stacks. Lateral homotypic fusion of adjacent stacks results in nonproductive transport of aggregates that can go through another round of Golgi posttranslational modifications (passive quality control). Heterotypic fusion allows for forward transport of the aggregates.

that would simultaneously result in the meandering, if not unidirectional transport, of the large cargoes from the *cis* to the *trans* face. This transfer process would require collisions between the individual stacks and therefore would be much reduced when the stacks are separated from one another, precisely as we report here, whether the separation is artificial (disrupting microtubule motility [nocodazole] or Golgi adhesion [Grasp KD]) or occurs naturally (fly cells).

Natural, oversized cargoes, such as collagen or chylomicrons, have first to be released from the ER (Fromme and Schekman, 2005). Using a cargo that can be artificially reaggregated within the Golgi allowed us to decouple ER exit from intra-Golgi trafficking, thereby assessing exclusively how oversized cargoes are transported across the Golgi. Because we have shown that natural cargoes such as collagen behave similarly, this suggests that the mechanism described here is physiologically relevant.

During the revision of our manuscript, Cutler and colleagues reported that the size of the Golgi determines copackaging of the von Willebrand factors (vWF), a giant cargo secreted by endothelial cells (Ferraro *et al.*, 2014). We considered whether the size of our soluble aggregates may be affected within nocodazole-induced ministacks. However, this was ruled out, because our EM data showed that the average size of soluble aggregates formed within nocodazole-induced Golgi stacks was 209 nm ± 90 nm (n = 38; Figure 2 and Supplemental Figure S5A) and very similar to the size reported previously within the full ribbon (Volchuk *et al.*, 2000).

We also considered that the presence of the soluble aggregates within the ministacks might alter the proper flow of endogenous cargo. However, this was ruled out, because mmp-2 secretion was unaltered by the presence of the aggregates within nocodazole-induced ministacks (Figure S6).

At first glance, the different Golgi morphologies encountered through evolution seem to correlate with the presence of large cargo. For instance, yeasts do not secrete collagen or, as far as we are aware, any similarly large polymeric cargo (note that chitin is secreted in a dispersed form and is assembled outside the cell; Cabib *et al.*, 2008), and they harbor single Golgi cisternae. Many insect cells harbor dispersed single stacks and secrete homologues of type IV mammalian collagens (network-forming collagens) (Yasothornsrikul *et al.*, 1997). Unlike type I, III, V, and XI collagens (fibril-forming collagens; Thyberg and Moskalewski, 1985; Ferraro *et al.*, 2014), type IV collagens harbor interruptions within the triple-helical domain repeats that are thought to introduce flexibility and instability in the triple helix (Bella *et al.*, 2006; Li *et al.*, 2007; Hwang *et al.*, 2010). However, it remains to be accurately determined to what extent such an increased flexibility would make collagen IV a better candidate than collagen I for loading into putative small transport carriers during intra-Golgi transport. Finally, mammalian cells secrete numerous fibril-forming collagen species that extensively aggregate within the cell, and it is these cells that display an extensive Golgi ribbon. "Professional" collagen/matrix-secreting cells, such as fibroblasts and osteoblasts, often contain a single elongated Golgi ribbon (Cho and Garant, 1985). These correlations broadly match the expectations of rim progression.

However, other observations do not match such predictions and incite us to temper our statement. Some algae have numerous separate Golgi stacks and yet efficiently secrete the macromolecule scale (Brown *et al.*, 1970). Other plants harboring individual Golgi stacks process aggregated cell wall precursors (Mollenhauer and Morre, 1991). Specific tissues of insect cells secrete dumpy (Wilkin *et al.*, 2000), a protein predicted to be 1 μm in size. These observations suggest that the ribbon structure is not absolutely required for the forward transport of oversized cargoes and that other mechanisms, such as cisternal maturation, may back up the lack of ribbon organization or complement the ribbon-dependent rim progression in mammals.

Interestingly, in our study, although the decrease of large cargo transport when ribbons were disrupted was substantial (~70%), this inhibition was never complete.

One possibility is that ribbon disruption is not complete. Paired Golgi stacks have been described within S2 cells and nocodazole-treated mammalian cells and could support such a possibility (Kondylis *et al.*, 2007). However, treatment with latrunculin B, which depolymerizes F-actin and triggers Golgi unpairing (Kondylis *et al.*, 2007), did not perturb the secretion of either small or large cargoes within S2 cells or nocodazole-treated HeLa cells (Figure S7). It remains unclear whether the paired Golgi are physically connected (Kondylis *et al.*, 2007), which would be required to favor rim progression; therefore it may be that Golgi pairing is not involved in protein transport and is exclusively involved in cell cycle regulation, as originally proposed (Kondylis *et al.*, 2007).

Another possibility is that a second process, such as cisternal progression, accounts for the residual transport of aggregates.

Considering all these aspects, we state that alteration of the ribbon structure promotes at least a delay in the transport of large cargoes, and we conclude that the ribbon structure facilitates the anterograde transport of oversized cargoes.

MATERIAL AND METHODS

Cell culture and transfection

HeLa cells were maintained at 37°C in 5% CO_2 in DMEM (Life Technologies, Carlsbad, CA) supplemented with 10% fetal bovine serum (FBS; Life Technologies). Saos-2 cells were maintained with the same media supplemented with ascorbate (25 μg/ml). The HT1080 human fibrosarcoma stable cell line expressing ssGFP-FM4-FCS-hGH was previously generated in our lab by Allen Volchuk (Volchuk *et al.*, 2000). HT1080 cells were grown similar to HeLa cells, except with the addition of 0.5 mg/ml geneticin and

50 U/ml penicillin-streptomycin (Life Technologies) to their medium. S2 cells were maintained at 25°C in Schneider's *Drosophila* medium (Life Technologies) supplemented with 10% FBS (Life Technologies). HeLa cells were transfected using Lipofectamine 2000 (Invitrogen, Carlsbad, CA) or RNAimax (Invitrogen) as recommended by the manufacturer. S2 cells were transfected using Effecten transfection reagent (Qiagen, Venlo, Netherlands) as recommended by the manufacturer. Saos-2 cells were transfected using electroporation (Nepa21 type II model from Nepa Gene, Chiba, Japan).

Plasmids and siRNA

pC4-ssGFPFM4hGH (mammalian cell expression plasmid) was published previously (Lavieu *et al.*, 2013). For expression within S2 cells, ssGFPFM4hGH was subcloned into the pENTR/SD/DTOPO vector (Invitrogen) and then into the pAW destination backbone vector from the Drosophila Gateway vector system (https://dgrc.cgb.indiana.edu). grasp55/65 siRNA sequences were reported previously (Lee *et al.*, 2014).

Secretion assay, SDS–PAGE, and immunoblot analysis

These experiments were performed as described previously (Lavieu *et al.*, 2013) with slight modifications. Cells were grown in six-well plates. For HeLa cells and Saos-2 cells, secretion experiments were performed in Hanks' balanced salt solution (HBSS; Life Technologies) supplemented with 0.1% FBS (Life Technologies) and 100 µg/ml CHX (Sigma-Aldrich, St. Louis, MO). When required, we used nocodazole (Sigma-Aldrich) at 1 µg/ml. For S2 cells, HBSS was replaced with Schneider's *Drosophila* medium. The disaggregating drug (D/D solubilizer from Clontech, Mountain View, CA) was used at 1 µM. Incubations were performed at 10, 16, 20, 32, and 37°C, using temperature-controlled incubators. Chase media were collected and precipitated overnight at 4°C with 10% trichloroacetic acid (TCA). After centrifugation, TCA pellets were washed with acetone before being resuspended in loading buffer and analyzed by immunoblotting. Cells were washed, detached, and collected by centrifugation. Pellets were resuspended in loading buffer. Extracted proteins were first separated in SDS–polyacrylamide gels and then transferred onto nitrocellulose membranes for immunoblotting. After being blocked with fat-free milk, the membranes were incubated with appropriate primary antibodies. We used anti-GFP (Roche, Basel, Switzerland), anti-collagen I (SP1.D8 from the Developmental Studies Hybridoma Bank, Iowa City, IA), anti-Grasp55 (Proteintech, Iowa City, IA), anti-Grasp65 (Santa Cruz Biotechnology, Dallas, TX), anti-GAPDH (Sigma-Aldrich), anti-actin (Cell Signaling Technology, Danvers, MA), and anti-MMP2 (Cell Signaling). Primary antibodies were detected by chemiluminescence using horseradish peroxidase–conjugated secondary antibodies. Fluorographs were quantitatively scanned using imageJ software.

Confocal and STED imaging

Cells were grown on glass coverslips in 24-well plates and were fixed for 10 min with 4% paraformaldehyde (PFA) before being triton permeabilized and incubated with the appropriate antibodies. We used anti-Grasp55 (Proteintech), anti-gpp130 (Covance, Princeton, NJ), anti-p230 (BD Biosciences, San Jose, CA), anti–collagen I (SP1.D8 from Developmental Studies Hybridoma Bank and Abcam), anti-dGm130 (Abcam, Cambridge, England), and anti-dG245 (a gift from S. Munro, Cambridge University). We used appropriate secondary antibodies coupled with Alexa Fluor 488 or Alexa Fluor 546 (Invitrogen) or ATTO647N (Active Motif, Carlsbad, CA).

Confocal images were obtained using a Zeiss LSM510 confocal microscope. Two-color STED images were acquired using a Leica TCS STED microscope. The dyes Star520P (Nizamov *et al.*, 2012) and Star635P (Wurm *et al.*, 2012) (both from Abberior [Göttingen, Germany]) were excited with 532-nm and 640-nm pulsed diode lasers, respectively. For depletion, a tunable, mode-locked Ti:Sapphire laser was used (760 nm for Star520SXP and 770 nm for Star635P). Imaging was performed with a 100×/1.4 NA oil-immersion objective lens. Fluorescence was split by a dichroic mirror (650-nm long-pass), band-pass filtered (FF01-685/40 for 640-nm excitation or FF01-582/75 for 532-nm excitation), and detected by avalanche photodiodes (APD1 for Star520SXP and APD2 for Star635P). Images were then smoothed with a 0.7 pixel full-width half-maximum Gaussian filter using ImageJ software.

Images were analyzed using Zeiss LSM510 software or using ImageJ (colocalization finder). Images were analyzed using Zeiss LSM510 software or using ImageJ (colocalization finder plug-in).

Statistical analysis

Analyses were performed with StatPlus software. A two-tailed unpaired *t* test type was used to determine *p* values. *N* (number of individual experiments) and *n* (number of objects [ministacks]) are noted in the figure legends.

Electron microscopy

For conventional EM, cells were fixed with 2% glutaraldehyde, buffered with 0.1 M sodium phosphate (pH 7.4), detached from their substrate, postfixed with osmium tetroxide, stained with uranyl acetate, dehydrated in ethanol, and embedded in Epon.

ACKNOWLEDGMENTS

We thank Sean Munro (Cambridge University) for the gift of the G245 antibody. Thanks to Xinran Liu and Morven Graham for their EM guidance and to Joerg Bewesdorf for access to the Leica TCS STED microscope. We thank Florian Wilfling, Nora Kory, and Huajin Wang (from Tobias Walther's lab) for sharing S2 cell–related reagents and for their guidance with the insect cell system. Thanks to Daniel Saint-Johnston for pointing out the case of the dumpy protein. We thank Abberior for sharing their valuable STED dyes. F.B. is supported by an American-Italian Cancer Foundation postdoctoral research fellowship. This investigation was supported by the National Institutes of Health under a Ruth L. Kirschstein National Research Service Award (F32 GM 101777 to M.H.D.).

REFERENCES

Bella J, Liu J, Kramer R, Brodsky B, Berman HM (2006). Conformational effects of Gly-X-Gly interruptions in the collagen triple helix. J Mol Biol 362, 298–311.

Brown RM Jr, Franke WW, Kleinig H, Falk H, Sitte P (1970). Scale formation in chrysophycean algae. Cellulosic I and noncellulosic wall components made by the Golgi apparatus. J Cell Biol 45, 246–271.

Cabib E, Farkas V, Kosik O, Blanco N, Arroyo J, McPhie P (2008). Assembly of the yeast cell wall. Crh1p and Crh2p act as transglycosylases in vivo and in vitro. J Biol Chem 283, 29859–29872.

Cho MI, Garant PR (1985). Effects of L-azetidine-2-carboxylic acid on matrix secretion and Golgi structure in fibroblasts and osteoblasts of the mouse. Anat Rec 212, 232–238.

Cole NB, Sciaky N, Marotta A, Song J, Lippincott-Schwartz J (1996). Golgi dispersal during microtubule disruption: regeneration of Golgi stacks at peripheral endoplasmic reticulum exit sites. Mol Biol Cell 7, 631–650.

Dejgaard SY, Murshid A, Dee KM, Presley JF (2007). Confocal microscopy-based linescan methodologies for intra-Golgi localization of proteins. J Histochem Cytochem 55, 709–719.

Feinstein TN, Linstedt AD (2008). GRASP55 regulates Golgi ribbon formation. Mol Biol Cell 19, 2696–2707.
Ferraro F, Kriston-Vizi J, Metcalf DJ, Martin-Martin B, Freeman J, Burden JJ, Westmoreland D, Dyer CE, Knight AE, Ketteler R, *et al.* (2014). A two-tier Golgi-based control of organelle size underpins the functional plasticity of endothelial cells. Dev Cell 29, 292–304.
Franzusoff A, Redding K, Crosby J, Fuller RS, Schekman R (1991). Localization of components involved in protein transport and processing through the yeast Golgi apparatus. J Cell Biol 112, 27–37.
Fromme JC, Schekman R (2005). COPII-coated vesicles: flexible enough for large cargo? Curr Opin Cell Biol 17, 345–352.
Glick BS, Luini A (2011). Models for Golgi traffic: a critical assessment. Cold Spring Harb Perspect Biol 3, a005215.
Griffiths G, Fuller SD, Back R, Hollinshead M, Pfeiffer S, Simons K (1989). The dynamic nature of the Golgi complex. J Cell Biol 108, 277–297.
Harwood R, Grant ME, Jackson DS (1976). The route of secretion of procollagen. The influence of αα′-bipyridyl, colchicine and antimycin A on the secretory process in embryonic-chick tendon and cartilage cells. Biochem J 156, 81–90.
Hell SW, Wichmann J (1994). Breaking the diffraction resolution limit by stimulated emission: stimulated-emission-depletion fluorescence microscopy. Opt Lett 19, 780–782.
Hwang ES, Thiagarajan G, Parmar AS, Brodsky B (2010). Interruptions in the collagen repeating tripeptide pattern can promote supramolecular association. Protein Sci 19, 1053–1064.
Kondylis V, Rabouille C (2003). A novel role for dp115 in the organization of tER sites in *Drosophila*. J Cell Biol 162, 185–198.
Kondylis V, van Nispen tot Pannerden HE, Herpers B, Friggi-Grelin F, Rabouille C (2007). The Golgi comprises a paired stack that is separated at G2 by modulation of the actin cytoskeleton through Abi and Scar/WAVE. Dev Cell 12, 901–915.
Ladinsky MS, Mastronarde DN, McIntosh JR, Howell KE, Staehelin LA (1999). Golgi structure in three dimensions: functional insights from the normal rat kidney cell. J Cell Biol 144, 1135–1149.
Lavieu G, Zheng H, Rothman JE (2013). Stapled Golgi cisternae remain in place as cargo passes through the stack. eLife 2, e00558.
Lee I, Tiwari N, Dunlop MH, Graham M, Liu X, Rothman JE (2014). Membrane adhesion dictates Golgi stacking and cisternal morphology. Proc Natl Acad Sci USA 111, 1849–1854.
Li Y, Brodsky B, Baum J (2007). NMR shows hydrophobic interactions replace glycine packing in the triple helix at a natural break in the (Gly-X-Y) n repeat. J Biol Chem 282, 22699–22706.
Mironov AA, Beznoussenko GV, Nicoziani P, Martella O, Trucco A, Kweon HS, Di Giandomenico D, Polishchuk RS, Fusella A, Lupetti P, *et al.* (2001). Small cargo proteins and large aggregates can traverse the Golgi by a common mechanism without leaving the lumen of cisternae. J Cell Biol 155, 1225–1238.
Mironov AA, Sesorova IV, Beznoussenko GV (2013). Golgi's way: a long path toward the new paradigm of the intra-Golgi transport. Histochem Cell Biol 140, 383–393.
Mollenhauer HH, Morre DJ (1991). Perspectives on Golgi apparatus form and function. J Electron Microsc Tech 17, 2–14.
Nizamov S, Willig KI, Sednev MV, Belov VN, Hell SW (2012). Phosphorylated 3-heteroarylcoumarins and their use in fluorescence microscopy and nanoscopy. Chemistry 18, 16339–16348.
Pellett PA, Dietrich F, Bewersdorf J, Rothman JE, Lavieu G (2011). Two-color STED microscopy in living cells. Biomed Opt Expr 2, 2364–2374.
Pellett PA, Dietrich F, Bewersdorf J, Rothman JE, Lavieu G (2013). Inter-Golgi transport mediated by COPI-containing vesicles carrying small cargoes. eLife 2, e01296.
Pfeffer SR (2010). How the Golgi works: a cisternal progenitor model. Proc Natl Acad Sci USA 107, 19614–19618.
Puthenveedu MA, Bachert C, Puri S, Lanni F, Linstedt AD (2006). GM130 and GRASP65-dependent lateral cisternal fusion allows uniform Golgi-enzyme distribution. Nat Cell Biol 8, 238–248.
Rabouille C, Kondylis V (2007). Golgi ribbon unlinking: an organelle-based G2/M checkpoint. Cell Cycle 6, 2723–2729.
Ricard-Blum S (2011). The collagen family. Cold Spring Harb Perspect Biol 3, a004978.
Rogalski AA, Bergmann JE, Singer SJ (1984). Effect of microtubule assembly status on the intracellular processing and surface expression of an integral protein of the plasma membrane. J Cell Biol 99, 1101–1109.
Saito K, Chen M, Bard F, Chen S, Zhou H, Woodley D, Polischuk R, Schekman R, Malhotra V (2009). TANGO1 facilitates cargo loading at endoplasmic reticulum exit sites. Cell 136, 891–902.
Schill H, Nizamov S, Bottanelli F, Bierwagen J, Belov VN, Hell SW (2013). 4-Trifluoromethyl-substituted coumarins with large Stokes shifts: synthesis, bioconjugates, and their use in super-resolution fluorescence microscopy. Chemistry 19, 16556–16565.
Thyberg J, Moskalewski S (1985). Microtubules and the organization of the Golgi complex. Exp Cell Res 159, 1–16.
Trucco A, Polishchuk RS, Martella O, Di Pentima A, Fusella A, Di Giandomenico D, San Pietro E, Beznoussenko GV, Polishchuk EV, Baldassarre M, *et al.* (2004). Secretory traffic triggers the formation of tubular continuities across Golgi sub-compartments. Nat Cell Biol 6, 1071–1081.
Van De Moortele S, Picart R, Tixier-Vidal A, Tougard C (1993). Nocodazole and Taxol affect subcellular compartments but not secretory activity of GH3B6 prolactin cells. Eur J Cell Biol 60, 217–227.
Volchuk A, Amherdt M, Ravazzola M, Brugger B, Rivera VM, Clackson T, Perrelet A, Sollner TH, Rothman JE, Orci L (2000). Megavesicles implicated in the rapid transport of intracisternal aggregates across the Golgi stack. Cell 102, 335–348.
Wilkin MB, Becker MN, Mulvey D, Phan I, Chao A, Cooper K, Chung HJ, Campbell ID, Baron M, MacIntyre R (2000). *Drosophila* dumpy is a gigantic extracellular protein required to maintain tension at epidermal-cuticle attachment sites. Curr Biol 10, 559–567.
Wurm CA, Kolmakov K, Göttfert F, Ta H, Bossi M, Schill H, Berning S, Jakobs S, Donnert G, Belov VN, *et al.* (2012). Novel red fluorophores with superior performance in STED microscopy. Opt Nanoscopy 1, 7–17.
Xiang Y, Zhang X, Nix DB, Katoh T, Aoki K, Tiemeyer M, Wang Y (2013). Regulation of protein glycosylation and sorting by the Golgi matrix proteins GRASP55/65. Nat Commun 4, 1659–1670.
Yasothornsrikul S, Davis WJ, Cramer G, Kimbrell DA, Dearolf CR (1997). *viking*: identification and characterization of a second type IV collagen in *Drosophila*. Gene 198, 17–25.